# Self-Assembly Characteristics of a Crystalline–Amorphous Diblock Copolymer in Nanoscale Thin Films

**ARTICLE** *in* MACROMOLECULES · OCTOBER 2013

Impact Factor: 5.8 · DOI: 10.1021/ma401440y

Macromolecules

Article

pubs.acs.org/Macromolecules

# Self-Assembly Characteristics of a Crystalline−Amorphous Diblock Copolymer in Nanoscale Thin Films

Young Yong Kim,[†,∥] Byungcheol Ahn,[†,∥] Seokpil Sa,[‡,∥] Manseong Jeon,[‡] Stephan V. Roth,[§] Sang Youl Kim,*[,‡] and Moonhor Ree*[,†]

[†]Division of Advanced Materials Science, Department of Chemistry, Pohang Accelerator Laboratory, Polymer Research Institute, Center for Electro-Photo Behaviors in Advanced Molecular Systems, and BK School of Molecular Science, Pohang University of Science and Technology, Pohang 790-784, Republic of Korea

[‡]Department of Chemistry, Korea Advanced Institute of Science and Technology, Daejeon 305-701, Republic of Korea

[§]HASYLAB, Deutsches Elektronen Synchrotron, Notkestr. 85, D-22607 Hamburg, Germany

Supporting Information

**ABSTRACT:** A diblock copolymer of crystalline polyethylene (PE) and amorphous poly(methyl methacrylate) (PMMA), $PE_{69}$-*b*-$PMMA_{92}$, was synthesized; this polymer is thermally stable up to 270 °C. The morphological structures of thermally annealed nanoscale thin films of the copolymer were investigated in detail at various temperatures by using in-situ grazing incidence X-ray scattering (GIXS) with a synchrotron radiation source. Quantitative GIXS analysis found that the PE and PMMA blocks undergo phase separation to produce a vertically oriented hexagonal PE cylinder structure in the PMMA matrix that is very stable up to around 100 °C (which is the onset temperature of PE crystal melting and PMMA glass transition); over the range 100−200 °C, slight variations with temperature in the cylinders' dimensions and orientation were observed. Furthermore, the PE block chains of the cylinder phase crystallize and undergo crystal growth along the cylinders' long axes; however, these lamellar crystals do not stack properly because of the limited space along the cylinders' short axes. As a result, the overall crystallinity is very low. The crystallization of the PE block chains in the diblock copolymer thin film is severely restricted in the diblock architecture by the confinement effects of the limited cylinder space and the anchoring of one end of the PE chain to the cylindrical wall interface. Surprisingly, however, in a nanoscale thin film the PE homopolymer forms a highly ordered lamellar structure; the lamellae are well stacked along the out-of-plane of the film, even though the crystallization is confined by the air and substrate interfaces. This well-ordered and oriented lamellar structural morphology does not arise in melt-crystallized PE bulk specimens.

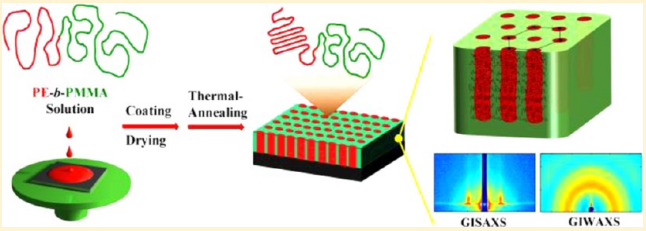


## INTRODUCTION

Block copolymers have attracted considerable attention because they form various kinds of microphase-separated morphologies with dimensions of a few nanometers to hundreds of nanometers, depending on the block components, compositions, and molecular weights.[1−3] Block copolymers are considered promising materials for nanometer-scale device applications because their properties can be facilely tuned through modification of their chemical structures, which means that well-ordered periodic structures can be constructed spontaneously. Thus, much research effort has focused on the development of block copolymers with various functionalities in order to achieve well-defined and ordered microphase-separated morphologies.[3]

In particular, the interest in crystalline−amorphous block copolymers has increased because they can exhibit properties of both crystalline and amorphous polymers.[4] A number of crystalline polymers are widely used in various fields because of their mechanical toughness, low permeability, and high stability. Further, various kinds of functional polymeric materials, and in particular functional nanostructured materials with excellent mechanical performance, can easily be synthesized by modifying amorphous polymers with functional moieties without affecting their mechanical properties. In nanostructured block copolymers, the crystalline blocks are confined within nanodomains, which can alter the crystallization behavior. Thus, there have been some attempts to investigate the crystallization behaviors of block copolymers under such confinement conditions.[5−7] However, studies of the crystallization behaviors of crystalline−amorphous block copolymers have been performed mostly for bulk states.[5,6] Functional nanostructured block polymers have attracted attention as a novel class of polymers because of their potential applications in nanoscale thin-film form in microelectronic, optical, and optoelectronic devices.[8] The structures of such block copolymer thin films can be significantly different from those of the bulk because their molecular configuration and

**Received:** July 9, 2013
**Revised:** September 16, 2013
**Published:** October 3, 2013

  

**Scheme 1. Synthetic Route for the $PE_{69}$-*b*-$PMMA_{92}$ Diblock Copolymer**

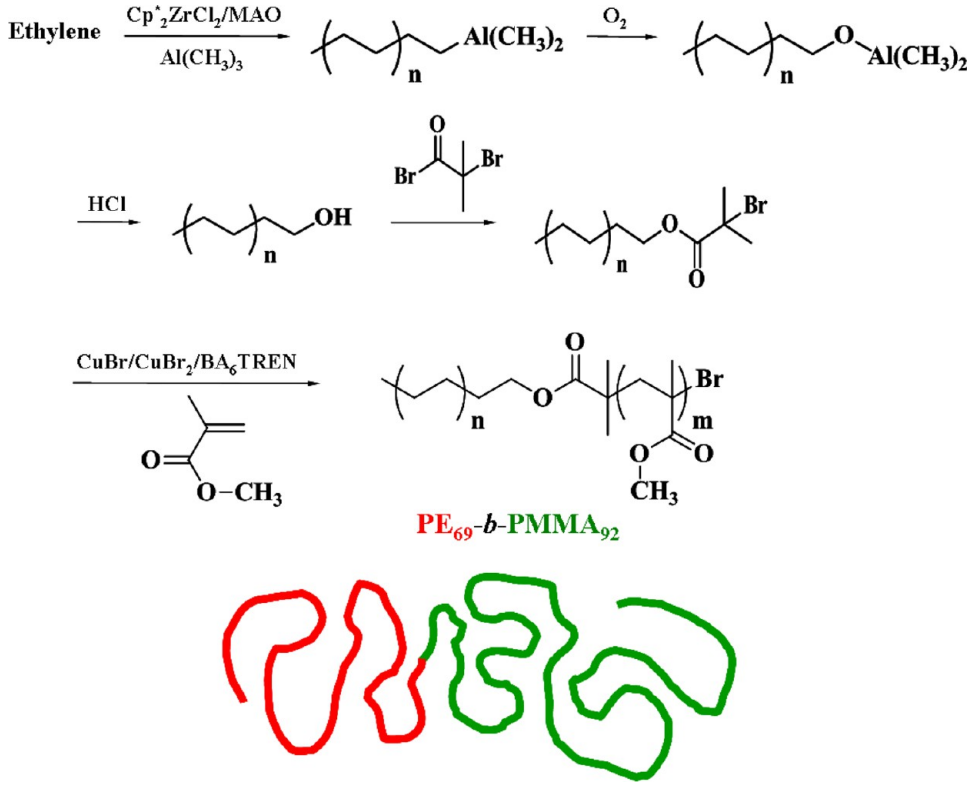


structural order can be affected by their interfaces with substrates and the air or vacuum. Moreover, the crystallization behaviors within the confined nanodomains of such thin films can be significantly different from those of the bulk. Thus, it is important to investigate the nanostructures and crystallization behaviors of crystalline−amorphous block copolymer thin films.

In this study, we synthesized a diblock copolymer composed of crystalline polyethylene (PE) block with an average degree of polymerization $\overline{DP}$ of 69 and amorphous poly(methyl methacrylate) (PMMA) block with $\overline{DP}$ = 92 ($PE_{69}$-*b*-$PMMA_{92}$). Nanoscale thin films of $PE_{69}$-*b*-$PMMA_{92}$ were prepared on silicon substrates via spin-coating and subsequent drying, followed by thermal annealing in order to produce phase-separated domains. The structures and crystallization behaviors of the thin films were investigated during heating and cooling by using synchrotron grazing incidence X-ray scattering (GIXS). In addition, differential scanning calorimetry (DSC) analysis was conducted.

## EXPERIMENTAL SECTION

A diblock copolymer of polyethylene (PE) and poly(methyl methacrylate) (PMMA) was prepared via sequential polymerization combined with ethylene polymerization with chain transfer to aluminum and atom transfer radical polymerization of methyl methacrylate, according to the reported procedure in the literature.[9] The simplified synthesis procedure is given in Scheme 1. For the synthesized block copolymer, the molecular weights of the PE and PMMA blocks were determined to be 1930 ($\overline{DP}$ = 69) and 8750 ($\overline{DP}$ = 92), respectively, from the proton nuclear magnetic resonance ($^1$H NMR) spectra measured using a Bruker 400 MHz spectrometer (Bruker, Rheinstetten, BW, Germany). From the molecular weight data, the volume fractions of the PE and PMMA blocks were estimated to be 18.1% and 81.9%, respectively. The diblock copolymer product was further determined to have a number-averaged molecular weight $\bar{M}_n$ of 14 200 and a polydispersity index PDI of 1.37 by using gel permeation chromatography (GPC). In addition, a PE homopolymer was synthesized in similar manner as the diblock copolymer was synthesized. The obtained PE homopolymer was measured to have $\bar{M}_n$ = 1900 and PDI = 1.82 by GPC analysis. The GPC measurements were conducted at room temperature using a Viscotek T60A gel permeation chromatography (GPC) system equipped with two PL Mixed-C columns; a refractive index detector in a Viscotek TDA302 triple detector array was employed. Chlorobenzene was used as an eluent. The molecular weights of the polymers were calculated relative to PMMA homopolymer standards (Varian EasiVial, Varian Polymer Laboratories, Amherst, MA). In addition, a PMMA polymer ($\bar{M}_n$ = 12 500 and PDI = 1.04) was purchased from Aldrich Chemicals (St. Louis, MO).

Thermal stabilities of the obtained polymers were examined with a ramping rate of 5.0 °C/min over the temperature range of 25−600 °C under a nitrogen atmosphere by thermogravimetry analysis (TGA) using a thermal analyzer (TG/DTA 6300, Seiko, Tokyo, Japan). In addition, DSC analysis was carried out with a ramping rate of 5.0 °C/min in a nitrogen atmosphere over the temperature range of 25−200 °C using a calorimeter (model DSC-220CU, Seiko, Tokyo, Japan).

The diblock copolymer product was dissolved in hot chlorobenzene and filtered using disposable syringe equipped with PTFE filter of pore size 1.0 $\mu$m, producing a 1.0 wt % solution. In the same manner, a 0.5 wt % solution of the PE homopolymer was prepared. These filtered solutions were readily spin-casted on silicon substrates and dried under vacuum at room temperature for 24 h. Some of the polymer film samples were further thermally annealed under vacuum at 170 °C for 48 h. Then, the thermally annealed polymer films were slowly cooled to room temperature with a rate of 1.0 °C/min to give enough time for crystallization of the PE block or PE homopolymer. The obtained polymer thin films were determined to have a thickness of around 70 nm, using a spectroscopic ellipsometer (model M-2000, Woollam, Lincoln, NE).

GIXS measurements were conducted at the 3C and 4C beamlines[10,11] of the Pohang Accelerator Laboratory, Pohang University of Science & Technology, Pohang, Korea, and the P03 beamline of PETRA-III, HASYLAB, Deutsches Elektronen Synchrotron, Hamburg, Germany. The samples were measured at a sample-to-detector distance (SDD) of


dx.doi.org/10.1021/ma401440y | *Macromolecules* 2013, 46, 8235−8244

2270 mm for grazing incidence small-angle scattering (GISAXS) and 127 mm for wide grazing incidence wide-angle scattering (GIWAXS). Scattering data were typically collected for 30−60 s using an X-ray radiation source of $\lambda = 0.138$ nm ($\lambda$, wavelength) with a two-dimensional (2D) charge-coupled detector (CCD) (Roper Scientific, Trenton, NJ). The incidence angle $\alpha_i$ of the X-ray beam was set at 0.160°, which is between the critical angle of the polymer thin film and the silicon substrate ($\alpha_{c,f}$ and $\alpha_{c,s}$). In the case of in-situ GIXS measurements, a rate of 2.0°/min was employed on heating and subsequent cooling run. Scattering angles were corrected according to the positions of the X-ray beams reflected from the silicon substrate with respect to precalibrated polystyrene-*b*-polyethylene-*b*-polybutadiene-*b*-polystyrene block copolymer or silver behenate powder (TCI, Tokyo, Japan). Aluminum foil pieces were applied as a semitransparent beam stop because the intensity of the specular reflection from the substrate is much stronger than the intensity of GIXS near the critical angle.

## RESULTS AND DISCUSSION

The $PE_{69}$-*b*-$PMMA_{92}$ diblock copolymer was found to undergo a two-step degradation, as shown in Figure 1a. The first step of the degradation begins around 270 °C (= $T_d$, the degradation temperature), and the second step of the degradation begins around 340 °C. The extent of degradation in the first step is less than that in the second step. Taking into consideration these results and the diblock copolymer's chemical structure, the first step of degradation is attributed to the ester-linked side groups in the PMMA block, and the second step of degradation is attributed to the disintegration of the backbones in the PE and PMMA blocks.

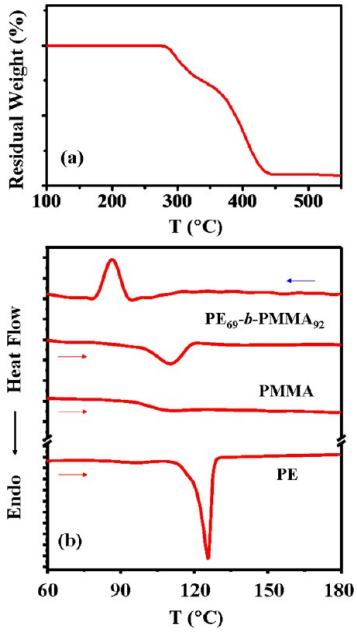


**Figure 1.** (a) TGA thermogram of the $PE_{69}$-*b*-$PMMA_{92}$ diblock copolymer and (b) DSC thermograms of PE homopolymer, PMMA homopolymer, and $PE_{69}$-*b*-$PMMA_{92}$ diblock copolymer.

Figure 1b shows representative DSC thermograms of the diblock copolymer and the homopolymers, which were measured at a rate of 5.0 °C/min during cooling from the melt state at 200 °C and subsequent heating. In the heating run, there is a strong endothermic peak for the PE homopolymer over the temperature range 117−129 °C, which corresponds to the melting of the crystals formed in the sample during cooling from the melt; the peak maximum of the crystal melting transition is 125 °C. The PMMA homopolymer produces only a weak, broad endothermic peak over the range 92−113 °C, which corresponds to the glass transition. Taking into account the PE homopolymer's crystal melting and the PMMA homopolymer's glass transition, the diblock copolymer is expected to exhibit a glass transition and crystal melting over the range 90−130 °C. Surprisingly, however, in the heating run the diblock copolymer produces a single broad endothermic peak over the range 98−120 °C. The heat of fusion of this endothermic peak is much stronger than that of the glass transition of the PMMA homopolymer but much weaker than that of the crystal melting transition of the PE homopolymer. The crystallization of the PE block chains in the diblock copolymer is evident in the DSC thermogram measured during cooling from the melt. The crystallization exothermic peak is present in the range 94−78 °C. Before the appearance of this exothermic peak, a weak transition is discernible in the region 112−94 °C. This weak and broad transition might be related to the glass transition of the PMMA block component. These results show that the single endothermic peak of the diblock copolymer in the DSC thermogram is due to the partial overlap between the glass transition of the PMMA block and the crystal melting of the PE block. The PE crystal melting temperature in the diblock copolymer is much lower than that of the PE homopolymer. Moreover, the diblock copolymer sample was estimated to have only 10% crystallinity with respect to that (293 J/g) of perfect PE crystals.[12] This crystallinity is much lower than that (91%) of the PE homopolymer sample. Overall, the DSC analysis results indicate that small PE crystals are present in the diblock copolymer sample.

Synchrotron GIXS analysis (Figure 2e) was performed on films of the diblock copolymer and the PE homopolymer (approximately 70 nm thick) that had been thermally annealed at 170 °C for 48 h followed by slow cooling at a rate of 1.0 °C/min. Figure 2a shows a representative 2D GISAXS pattern for a thermally annealed diblock copolymer film at room temperature. From the scattering pattern, in-plane and out-of-plane scattering profiles were extracted, as shown in Figure 2c,d.

From the scattering pattern, in-plane and out-of-plane scattering profiles were extracted, as shown in Figure 2c,d. The in-plane scattering profile contains two scattering peaks at 0.46° and 0.78° ($2\theta_f$) with relative scattering vector lengths from the specular reflection position of 1 and $\sqrt{3}$, respectively. However, these two scattering peaks are not present in the out-of-plane scattering profile. These scattering characteristics suggest that in the film the PE and PMMA blocks have undergone phase separation and formed a hexagonally packed cylinder structure that is preferentially oriented along a direction normal to the film plane. The PE block is the minor component in the volume fraction. Thus, the cylinder domains consist of the phase-separated PE block phase and the matrix phase consists of PMMA blocks.

The properties of the phase-separated structure of the diblock copolymer film were examined by analyzing the above scattering pattern with the GIXS formula derived for a hexagonal cylinder structure model[13−16] (the details of this derivation are in the Supporting Information). The in-plane and out-of-plane scattering profiles were satisfactorily fitted with the GIXS formula. The obtained structural parameters are listed in Table 1. The PE cylinders were found to have a length $H$ of 56.0 nm, a radius $R$ of 4.3 nm, and an interdistance $d$ of 18.7 nm. The hexagonal cylinder structure was determined to have a second-order orientation factor $O_s$ of 0.922. This GIXS analysis


dx.doi.org/10.1021/ma401440y | *Macromolecules* 2013, 46, 8235−8244

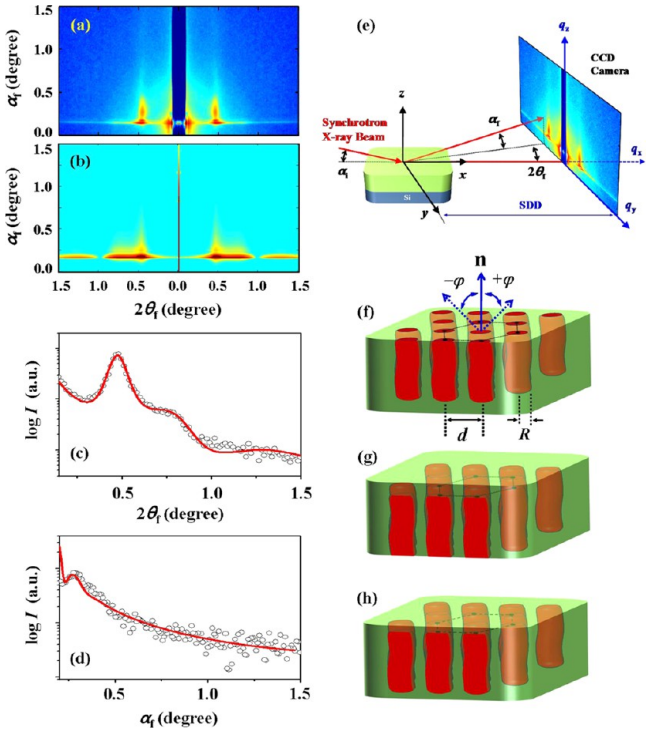


**Figure 2.** (a) 2D GISAXS pattern measured with $\alpha_i = 0.160°$ for the thermally annealed $PE_{69}$-*b*-$PMMA_{92}$ diblock copolymer thin film deposited on a silicon substrate. (b) 2D GISAXS pattern reconstructed for the diblock copolymer films by using the GIXS formula with the structural parameters in Table 1. (c) In-plane scattering profile extracted from the GISAXS pattern in (a) along the $2\theta_f$ direction at $\alpha_f = 0.174°$. (d) Out-of-plane scattering profile extracted from the GISAXS pattern in (b) along the $\alpha_f$ direction at $2\theta_f = 0.462°$. In (c) and (d), the black symbols are the measured data and the red lines are the scattering profile obtained by fitting the measured data with the GIXS formula. (e) Geometry of GISAXS: $\alpha_i$ is the incident angle at which the X-ray beam impinges on the film surface; $\alpha_f$ and $2\theta_f$ are the exit angles of the X-ray beam with respect to the film surface and to the plane of incidence, respectively, and $q_x$, $q_y$, and $q_z$ are the components of the scattering vector **q**. (f–h) Schematic representations of the hexagonally packed cylinder structure in the thermal-annealed diblock copolymer thin film composed of phase-separated PE cylinder domains. In (f), **n** is the orientation vector of the hexagonal cylinder structure, $\varphi$ is the polar angle between the **n** vector and the out-of-plane of the film, $d$ is the interdistance and the radius of cylinders, and $R$ is the radius of cylinder.

confirmed that in the nanoscale thin film there is a hexagonal cylinder structure preferentially oriented in the out-of-plane of the film. However, the determined $H$ value has a standard deviation $\sigma_H$ of 10.7 nm, which is not small. Thus, the maximum $H$ value is very close to the film thickness, but the mean and minimum $H$ values are relatively smaller than the film thickness. The determined $R$ value has a standard deviation $\sigma_R$ of 1.0 nm, which is not small either. Furthermore, the cylinders have a paracrystal distortion factor $g$, which is a measure of the positional distortion in the film plane, of 0.145, that is also not small. The orientation factor $O_s$ has a standard deviation $\sigma_\varphi$ of 2.97° in the mean polar angle $\bar{\varphi}$ between the orientation vector **n** of the hexagonal cylinder structure and the out-of-plane of the film. These results show that there is a certain level of disorder in the hexagonal PE cylinder structure formed in the diblock copolymer film in both the individual cylinders and their packing order and orientation. This disorder might be due in part to the crystallization in the PE cylinder domains and the bottom and top interfaces.

The structural parameters in Table 1 were used to reconstruct the 2D GISAXS image. The reconstructed scattering image is displayed in Figure 2b and is in good agreement with the experimental data. Based on these analysis results, three possible structural models were developed for the phase-separated morphology formed in the thermally annealed $PE_{69}$-*b*-$PMMA_{92}$ diblock copolymer films, as shown in Figure 2f–h. For the first structural model, the PE block components are anchored onto the top free surface and developed downward in the film as cylinders. In the second model, the PE block components are anchored onto the bottom substrate surface and developed upward in the film as cylinders. For the third model, the vertically oriented PE cylinders are developed in the film but could not reach to the bottom and top surfaces.

The vertically oriented hexagonal cylinder structure determined above is quite interesting, which is different from horizontally oriented hexagonal cylinder structures very often observed in thin films of common diblock copolymers.[2,15−17] PE is known to reveal a surface energy $E_s$ of 34 mJ/m$^2$ at room temperature,[18] which is relatively lower than that (41 mJ/m$^2$) of PMMA.[19] The $E_s$ value of PMMA is much closer to those (50 and 48 mJ/m$^2$) of silicon substrates without and with silicon oxide layer.[20] Considering these surface energy data, one can expect that the silicon substrate surface is covered predominantly with

**Table 1. Structural Parameters of Thermally Annealed Thin Films of $PE_{69}$-*b*-$PMMA_{92}$ As Obtained with Quantitative GISAXS Analysis**

| $T$ (°C) | $d^a$ (nm) | $R^b$ (nm) | $\sigma_R{}^c$ (nm) | $H^d$ (nm) | $\sigma_H{}^e$ (nm) | $g^f$ | $\bar{\varphi}^g$ (deg) | $\sigma_\varphi{}^h$ (deg) | $O_s{}^i$ |
|---|---|---|---|---|---|---|---|---|---|
| 25 | 18.7 | 4.3 | 1.0 | 56.0 | 10.7 | 0.145 | 0 | 2.97 | 0.922 |
| 80[j] | 18.7 | 4.3 | 1.3 | 56.0 | 10.8 | 0.145 | 0 | 3.11 | 0.919 |
| 94[j] | 18.9 | 4.4 | 1.3 | 55.6 | 10.8 | 0.145 | 0 | 3.31 | 0.914 |
| 100[j] | 18.9 | 4.5 | 1.5 | 54.5 | 11.0 | 0.148 | 0 | 3.82 | 0.902 |
| 150[j] | 19.2 | 4.7 | 1.8 | 52.5 | 11.2 | 0.161 | 0 | 4.25 | 0.892 |
| 170[j] | 19.0 | 4.7 | 2.0 | 51.8 | 11.5 | 0.165 | 0 | 4.46 | 0.869 |
| 180[j] | 19.0 | 4.7 | 2.0 | 50.1 | 11.5 | 0.175 | 0 | 4.67 | 0.882 |
| 190[j] | 19.0 | 4.7 | 2.0 | 48.4 | 11.6 | 0.185 | 0 | 5.73 | 0.857 |
| 200[j] | 18.3 | 4.7 | 2.0 | 44.0 | 11.8 | 0.197 | 0 | 5.94 | 0.853 |
| 30[k] | 18.3 | 4.5 | 1.9 | 50.5 | 11.5 | 0.180 | 0 | 4.67 | 0.882 |

[a]Center-to-center distance of the PE cylinders. [b]PE cylinder radius. [c]Standard deviation of the PE cylinder radius. [d]PE cylinder length. [e]Standard deviation of the PE cylinder length. [f]Paracrystal distortion factor of the interdistance between PE cylinders. [g]Mean polar angle between the orientation vector **n** of the hexagonal PE cylinder structure and the out-of-plane of the film. [h]Standard deviation of the polar angle $\varphi$ from the mean polar angle $\bar{\varphi}$. [i]Second-order orientation factor of the hexagonal PE cylinder structure. [j]Heating run. [k]Cooling run.


dx.doi.org/10.1021/ma401440y | *Macromolecules* 2013, 46, 8235−8244

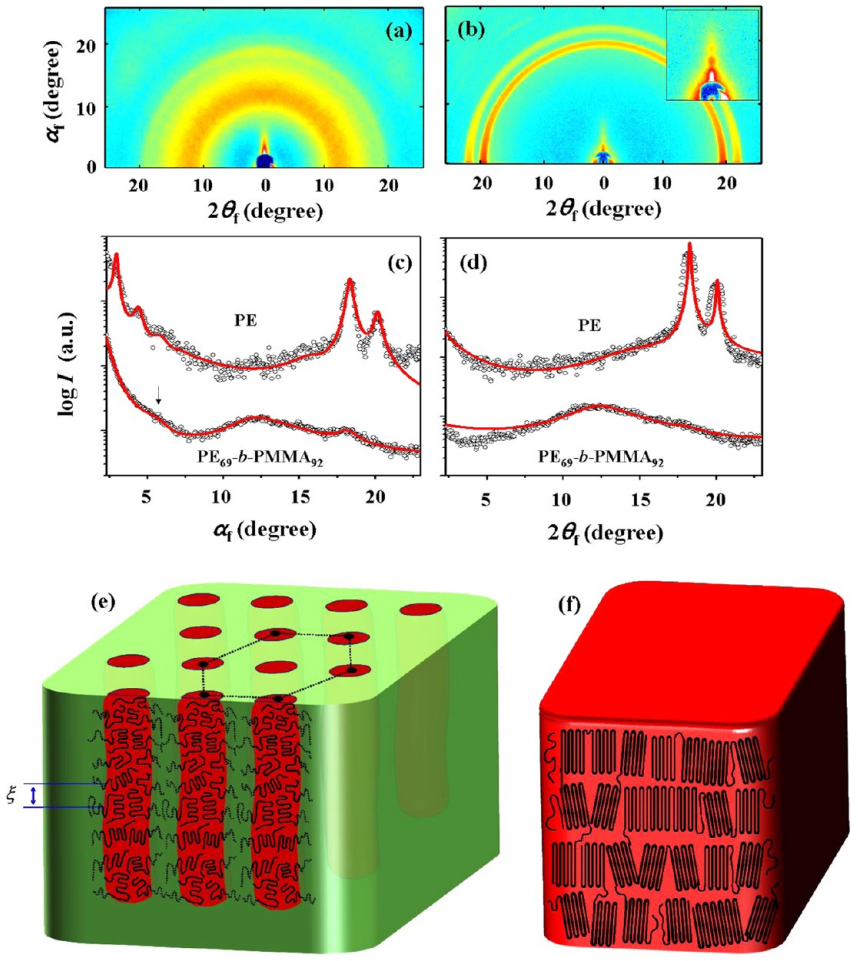


**Figure 3.** 2D GIWAXS patterns obtained with $\alpha_i = 0.160°$ for polymer thin films deposited on silicon substrates: (a) thermally annealed PE$_{69}$-*b*-PMMA$_{92}$ diblock copolymer film; (b) thermally annealed PE homopolymer film. The inset in (b) shows an enlargement of the scattering pattern in the small-angle region. (c) Out-of-plane scattering profiles extracted from the scattering patterns in (a) and (b) along the $\alpha_f$ direction at $2\theta_f = 0.0°$. (d) In-plane scattering profiles extracted from the scattering patterns in (a) and (b) along the $2\theta_f$ direction at $\alpha_f = 0.300°$. In (c) and (d), the black symbols are the measured data, and the red solid lines were obtained by fitting the data using the GIXS formula. Schematic representation of the PE crystals formed in the thermal-annealed films: (e) PE$_{69}$-*b*-PMMA$_{92}$ diblock copolymer; (f) PE homopolymer.

the PMMA block component rather than the PE block component, inducing horizontally oriented PE cylinder structure in the thin film. However, the diblock copolymer solution was prepared using chlorobenzene having $E_s = 33$ mJ/m$^2$,[21] which is almost same with that of PE. Thus, the solvent can play as a moderator for both the block components to contact to the bottom substrate surface through the polymer solution coating and subsequent drying process. As a result, the bottom substrate surface is covered in part by the PE block component. On the other hand, the PE block component is more preferred to the top (i.e., air or vacuum) surface compared to the PMMA block component. The as-cast films were found to reveal a featureless 2D GISAXS pattern, as shown in Figure S1a−c of the Supporting Information. A weak, broad scattering peak was clearly discernible in the in-plane scattering profile; such a scattering peak could not easily be discernible in the out-of-plane scattering profile. The scattering peak was determined to have a *d*-spacing of 18.2 nm. Moreover, the as-cast films revealed a scattering peak around 18.7° (*d*-spacing = 0.424 nm) (Figure S1d−f), which is one of the characteristic reflections from PE crystals,[22] in addition to a very broad scattering ring around 12.3°. These GIXS data inform that the block components of the PE$_{69}$-*b*-PMMA$_{92}$ polymer were found to undergo phase separation even in spin-coating and subsequent drying under vacuum at room temperature for 24 h. The phase-separated PE block phases in the as-cast film have a mean interdistance of 18.2 nm, which is close to the mean interdistance (18.7 nm) of the vertically oriented PE cylinders in the thermal-annealed film. Collectively, the PE block parts anchored onto the bottom and top surfaces may induce to build up PE cylinders vertically through post thermal annealing process. In particular, the post-thermal annealing process was conducted in vacuum at 170 °C for 48 h. Thus, the vertically oriented PE cylinders might be led predominantly by the PE block parts anchored onto the top vacuum surface (see the structural model in Figure 2f).

The thermal-annealed diblock copolymer films were further examined by using synchrotron GIWAXS analysis in order to obtain information about the structures of the crystals in the PE cylinder domains. A representative 2D GIWAXS pattern is displayed in Figure 3a; for comparison, a 2D GIWAXS pattern of a PE homopolymer film (which was prepared under the same conditions as the diblock copolymer films) is shown in Figure 3b. Their out-of-plane and in-plane scattering profiles are displayed in Figure 3c,d.

The PE homopolymer film produces three scattering peaks in the high angle region: at 15.9°, 18.4°, and 20.2°. The scattering


dx.doi.org/10.1021/ma401440y | *Macromolecules* 2013, 46, 8235−8244

**Table 2. Structural Parameters of Thermally Annealed Thin Films of the PE Homopolymer and the $PE_{69}$-*b*-$PMMA_{92}$ Diblock Copolymer As Obtained with Quantitative GIWAXS Analysis**

| thin film sample | $T$ (°C) | $d_{110}$[a] (nm) | $d_{200}$[b] (nm) | $g$[c] | $\overline{\varphi}$[d] (deg) | $\sigma_\varphi$[e] (deg) | $O_s$[f] | $L$[g] (nm) | $l_c$[h] (nm) | $l_a$[i] (nm) | $\xi$[j] (nm) |
|---|---|---|---|---|---|---|---|---|---|---|---|
| PE | 25 | 0.433 | 0.394 | 0.048 | 0 | 20 | 0.798 | 5.200 | 3.500 | 1.700 | |
| $PE_{69}$-*b*-$PMMA_{92}$ | 25 | 0.438 | – | 0.112 | 90 | 39 | 0.651 | | | | 1.400 |
| on heating | | | | | | | | | | | |
| | 95 | 0.423 | – | 0.137 | 90 | 45 | 0.613 | | | | 1.200 |
| | 100 | 0.439 | – | 0.195 | 90 | 67 | 0.495 | | | | |
| | 150 | | | | | | | | | | |
| | 200 | | | | | | | | | | |
| on cooling | | | | | | | | | | | |
| | 100 | | | | | | | | | | |
| | 70 | 0.435 | – | 0.172 | 90 | 58 | 0.539 | | | | |
| | 67 | 0.433 | – | 0.165 | 90 | 62 | 0.518 | | | | |
| | 50 | 0.427 | – | 0.165 | 90 | 51 | 0.577 | | | | |

[a] *d*-spacing of the {110} reflection from the PE crystal. [b] *d*-spacing of the {200} reflection from the PE crystal. [c] Paracrystal distortion factor of the PE crystal. [d] Mean polar angle between the orientation vector **n** of the PE crystal and the out-of-plane of the film. [e] Standard deviation of the polar angle $\varphi$ from the mean polar angle $\overline{\varphi}$. [f] Second-order orientation factor of the PE crystal. [g] Long period of the lamellar structure formed in the PE cylinders. [h] Thickness of the crystal layer in the lamellar structure. [i] Thickness of the amorphous layer in the lamellar structure. [j] *d*-spacing of the scattering peak at 5.7° along the $\alpha_f$ direction in Figure 3c.

peak at 15.9° (*d*-spacing = 0.498 nm) is weak, broad, and isotropic, which is typical of an amorphous halo. This scattering peak confirms that amorphous phase is present in a low fraction in the PE homopolymer film. In contrast, the two peaks at 18.4° and 20.2° are much stronger in intensity. These are typical peaks for PE crystals in an orthorhombic lattice and thus are assigned to the {110} and {200} reflections, respectively. Moreover, these scattering peaks are stronger in intensity along the in-plane of the film than along the out-of-plane of the film, which indicates that the *c*-axis of the orthorhombic PE crystals in the film is preferentially oriented along the out-of-plane of the film rather than along the film plane. Surprisingly, in the low-angle region the PE film produces four additional scattering peaks at 3.0°, 4.5°, 6.0°, and 7.3° along the out-of-plane of the film. Their relative scattering vector lengths from the specular reflection position are 1, 2, 3, and 4, respectively, which show that they arise from the same structural origin, namely lamellae stacked along the out-of-plane of the film. Thus, they can be assigned as the first-, second-, third-, and fourth-order reflections of the in-plane oriented lamellar structure. These scattering peaks were not detected along the in-plane of the film. The observation of these scattering peaks indicates that in the PE homopolymer film there is a highly ordered lamellar nanostructure with lamellae well stacked along the out-of-plane of the film, even though the PE thin film is confined by the air and substrate interfaces. Taking these results into account, the scattering pattern was analyzed quantitatively by using a GIXS formula derived by considering the lamellar structure, the orthorhombic lattice, and the amorphous halos (the details of the derivation are in the Supporting Information). As shown in Figure 3c,d, the out-of-plane and in-plane scattering profiles can be satisfactorily fitted with the GIXS formula. The determined structural parameters are listed in Table 2. The lamellar crystal structures were determined to have a long period $L$ of 5.200 nm, which consists of a crystal layer thickness $l_c$ of 3.500 nm and an amorphous layer thickness $l_a$ of 1.700 nm. For the amorphous layers, the polymer chains have a mean interdistance of 0.484 nm. For the lamellar crystals with an orthorhombic lattice, the {110} and {200} reflections have *d*-spacings of 0.433 and 0.394 nm, respectively, which are comparable to those of melt-crystallized bulk specimens of high molecular weight PE polymers.[22] The lamellar structure was confirmed to have an out-of-plane orientation ($O_s$ = 0.798; $\overline{\varphi}$ = 0°) with some distribution ($\sigma_\varphi$ = 20°); the *c*-axis of the orthorhombic crystals is preferentially oriented along the out-of-plane of the film. The paracrystal distortion factor $g$ (i.e., the positional distortion factor) of the lamellar structure is very low (0.048). Overall, the PE chains undergo self-assembly (i.e., crystallization) even in the 70 nm thick film confined by the silicon substrate and air interfaces, forming a highly ordered lamellar structure in which the lamellae are stacked along a direction normal to the film plane (i.e., a horizontally oriented lamellar structure). This highly ordered lamellar crystal structure with its highly preferential orientation is not easily obtained in common melt-crystallized PE specimens in bulk.

The diblock copolymer film produces two scattering peaks in the high angle region (Figure 3a,c). One peak at 12.1° (*d*-spacing = 0.656 nm) is very broad and isotropic but relatively strong in intensity. This isotropic scattering ring resembles that of the amorphous PMMA homopolymer and, therefore, can be assigned to the PMMA matrix in the diblock copolymer film. Because of this broad halo, the halo ring of the amorphous phase that is present at a certain fraction in the PE block phase, which is expected to appear around 15.9°, is not easily discerned. The peak at 18.1° is a typical scattering signal from PE crystals with an orthorhombic lattice that can be assigned to the {110} reflection. This peak is anisotropic in intensity. Its intensity is much stronger along the out-of-plane of the film than along the in-plane of the film. This anisotropic behavior is opposite to that observed for the PE homopolymer film. Furthermore, its overall intensity is much weaker than that of the PE homopolymer film. This peak's integrated intensity is only 14% of that for the PE homopolymer film. This ratio is consistent with that estimated from the heats of fusion (i.e., the crystallinities) in the DSC analysis above. Further, the {200} reflection is not easily discerned. In the low angle region, the diblock copolymer film produces an additional peak at 5.7° only along the out-of-plane of the film (Figure 3c). Taking into consideration these results, the scattering pattern was analyzed in detail by using the GIXS formula that was used for the scattering data analysis of the PE homopolymer films. The out-of-plane and in-plane scattering profiles were satisfactorily fitted with the GIXS formula (Figure 3c,d). The obtained structural parameters are listed in Table 2.


dx.doi.org/10.1021/ma401440y | *Macromolecules* 2013, 46, 8235−8244

The amorphous halo peak was determined to have a *d*-spacing of 0.656 nm, which is much larger than that of the amorphous layers in the lamellar crystal structure of the PE homopolymer film. This relatively large *d*-spacing value is attributed to the amorphous PMMA matrix and the amorphous PE phases in the PE cylinders. The orthorhombic crystals' {110} reflection has a *d*-spacing of 0.438 nm, which is slightly larger than that of the PE homopolymer film. This somewhat large *d*-spacing value shows that orthorhombic PE crystals form with less ordering in the diblock copolymer film. Moreover, the paracrystal distortion factor *g* (i.e., the positional distortion factor) of the orthorhombic crystals is larger (0.112) than that (0.048) of the crystals in the PE homopolymer film. The orthorhombic crystals' *c*-axis was found to have a preferential orientation along the in-plane of the film ($O_s$ = 0.651; $\bar{\varphi}$ = 90°), which is quite different from that of the PE homopolymer film. The in-plane orientation has a relatively wide distribution ($\sigma_\varphi$ = 39°). Considering this in-plane orientation characteristic of the orthorhombic crystals, one can easily imagine a lamellar crystal structure with lamellae stacked along the in-plane direction of the film (i.e., vertically oriented lamellar structure). However, no scattering signals due to such a vertical lamellar structure are present in the in-plane scattering profile (Figure 3d). This result suggests that lamellar crystal stacking is very limited or prohibited along the radial direction of the PE cylinder because of the small cylinder radius ($R$ = 4.3 nm); here it is noted that the cylinder radius is slightly smaller than the long period $L$ (5.20 nm) of the lamellar stacks formed in the PE homopolyer thin film discussed above. Instead, there is a weak and broad peak in the low-angle region of the out-of-plane scattering profile (see the peak marked with an arrow in Figure 3c), as mentioned above. This peak profile was analyzed by using a horizontal lamellar structure model and with a correlation function approach. The horizontal lamellar structure model analysis suggests a long period $L$ of only 1.400 nm consisting of a crystal layer thickness $l_c$ of 0.400 nm and an amorphous layer thickness $l_a$ of 1.000 nm. The correlation function approach suggests $L$ = 1.310 nm with $l_c$ = 0.590 nm and $l_a$ = 0.720 nm. These $l_c$ values (0.400−0.590 nm) correspond to only 2.5−4 chemical repeat units of the PE chain. Since the crystal melting endothermic peak was found to be at 98−120 °C in the DSC analysis, such $l_c$ values are unrealistically small. Thus, the weak, broad scattering peak at 5.7° in the out-of-plane scattering profile could originate from morphological components other than lamellar stacks, possibly components developed along the out-of-plane of the film (i.e., along the length of the PE cylinders). In conclusion, the scattering data analysis results show that in the diblock copolymer film lamellar crystals are poorly developed in the PE cylinder phases, which have a polymer chain axis that is preferentially aligned along the film plane (i.e., along the radial direction of the vertical PE cylinders), and their stacking is also limited by the confinement effects of the relatively small radii of the PE cylinders.

Here, the question arises as to the origin of the weak and broad scattering at 5.7° in the out-of-plane scattering profile. The PE block chains in the vertically oriented PE cylinders in the diblock copolymer film share an interface with the PMMA block chains via the cylindrical wall contact, as displayed in Figure 2f. Because of the confined diblock architecture, all the individual PE block chains have one end anchored to the cylindrical wall interface. Thus, the part of the PE chain near the cylindrical wall contact cannot be involved in self-assembly (i.e., crystallization) and, as a result, remains noncrystalline. The rest of the PE block chain can have relatively high mobility, as required by self-assembly, yet is likely to experience some restriction because it is anchored to the cylinder wall and consequently undergoes crystallization with some limitations. During the crystallization of the PE cylinder phase, crystals can grow more favorably along the long axes of the cylinders because there is more space in this direction than along the radial direction of the cylinders. These crystals growing along the long axes of the cylinders are likely to encounter neighboring growing crystals and thus experience some limits to further growth. As a result, morphological heterogeneity is likely to develop along both the cylinders' long axes and the cylinders' radial axes. Any scattering by the morphological heterogeneity generated along the cylinders' radial direction is likely to be very weak because the pass length of the X-ray beam is limited by the short cylinder radius and is thus hardly discernible. In contrast, any scattering of the morphological heterogeneity generated along the cylinders' long axes is likely to be discernible because of the relatively long pass length of the X-ray beam. Therefore, the scattering peak observed around 5.7° in the out-of-plane scattering profile might originate from such morphological heterogeneity generated along the cylinders' long axes. Considering the PE crystals' melting temperature and the {110} reflection intensity, the crystals are likely to have a mean interdistance along the cylinders' long axes larger than 1.400 nm (the *d*-spacing of the scattering peak at 5.7°). Therefore, the weak and broad scattering peak might be due to the mean interdistance $\xi$ of the aggregates of the PE blocks' noncrystalline parts with ends anchored to the cylinder wall interface (Figure 3e).

From the GIWAXS analysis results above, molecular structural models were developed for the vertically oriented PE cylinders in the thermally annealed $PE_{69}$-*b*-$PMMA_{92}$ diblock copolymer film and the thermally annealed PE homopolymer films, as shown in Figure 3e,f.

In-situ GIXS measurements were further conducted on the diblock copolymer films during heating up to 200 °C and subsequent cooling, in order to characterize their structural stability and to identify any possible phase transitions. In the GIWAXS pattern the {110} reflection peak of the PE crystals varies very little up to 95 °C but has weakened significantly by 100 °C; above 100 °C the {110} reflection peak is no longer discernible, which is due to the melting of the PE crystals (Figure 4a−e). The crystal melting indicated by the GIWAXS results is consistent with the DSC results discussed above. During this heating run, the *d*-spacing value of the {110} reflection varies little with temperature until the melting of the PE crystals (Table 2). However, the PE crystals' *g* and $\sigma_\varphi$ values increase significantly with temperature even below the melting temperature (Table 2). These results show that the crystals formed in the PE cylinder phases are stable until melting, but their positional movement and orientation distribution increase with increasing temperature, which might be due to the relatively high levels of thermal motion of the PE blocks and/or their segments in the amorphous phase. During the subsequent cooling run from the melt, the {110} reflection again appears around 70 °C, which indicates that crystals are being formed. The crystal formation indicated by the GIWAXS results is consistent with the DSC results discussed above. The {110} reflection increases in intensity with further decreases in the temperature (Figure 4f−j). Its *d*-spacing value returns to that of the film sample before the heating run (Table 2). However, the reformed crystals have higher *g* and $\sigma_\varphi$ values, which confirm that thermal annealing is necessary to improve the preferential orientation of the crystals formed in the PE cylinders of the diblock copolymer film.


dx.doi.org/10.1021/ma401440y | *Macromolecules* 2013, 46, 8235−8244

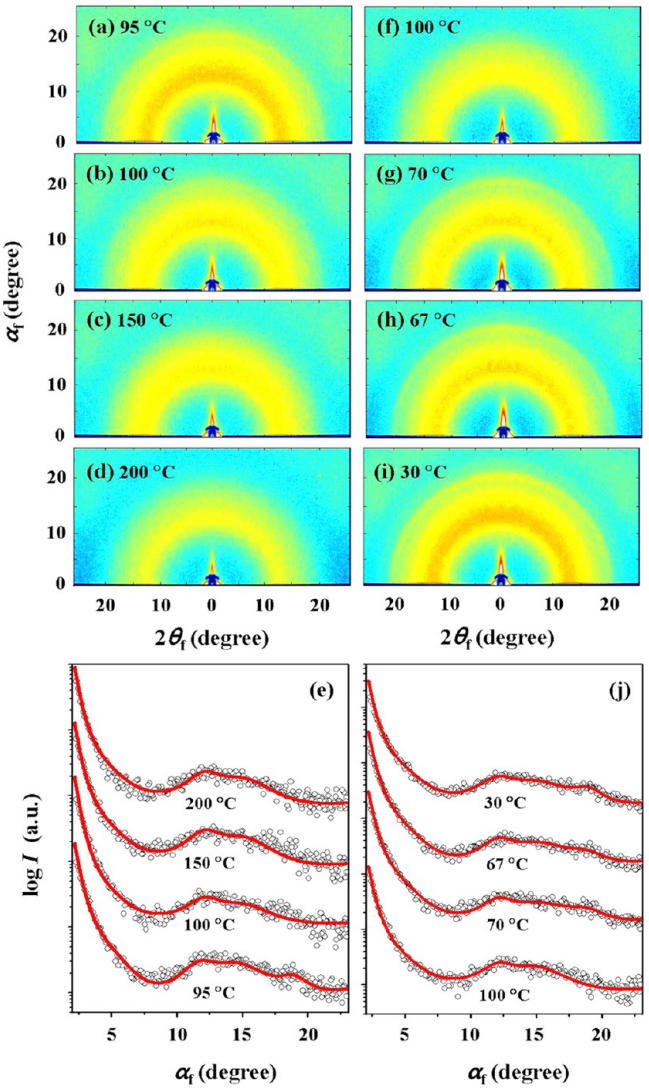


**Figure 4.** Representative 2D GIWAXS patterns obtained at $\alpha_i = 0.160°$ for thermally annealed $PE_{69}$-*b*-$PMMA_{92}$ diblock copolymer thin films deposited on silicon substrates during heating and subsequent cooling: (a) 95, (b) 100, (c) 150, and (d) 200 °C during heating; (f) 100, (g) 70, (h) 67, and (i) 30 °C during subsequent cooling. Out-of-plane scattering profiles extracted from the scattering patterns in (a–d) and (f–i) along the $\alpha_f$ direction at $2\theta_f = 0.0°$: (e) extracted from (a–d); (j) extracted from (f–i). In (e) and (j), the black symbols are the measured data and the red lines are the scattering profile obtained by fitting the measured data with the GIXS formula.

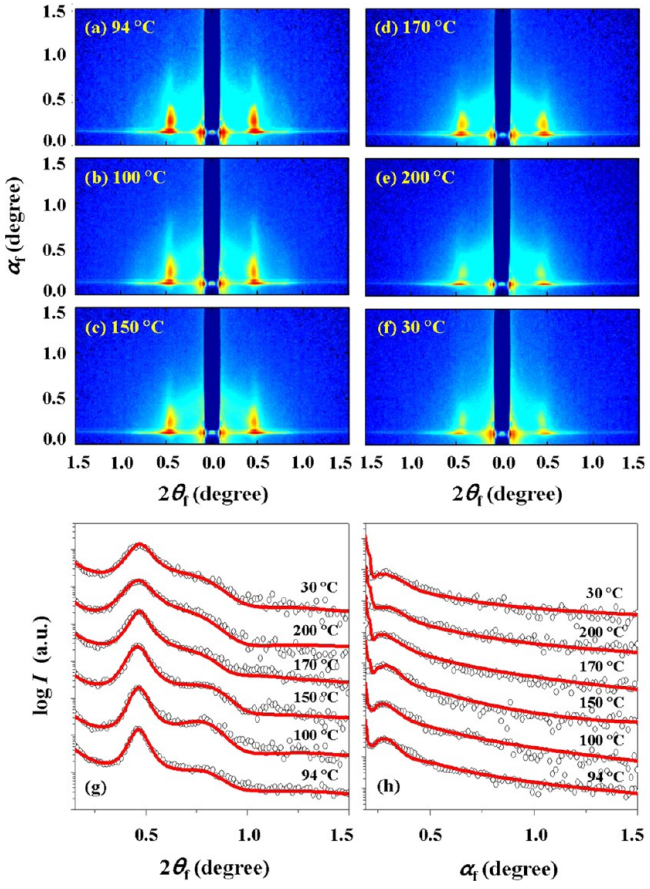


**Figure 5.** Representative 2D GISAXS patterns obtained at $\alpha_i = 0.160°$ for thermally annealed $PE_{69}$-*b*-$PMMA_{92}$ diblock copolymer thin films deposited on silicon substrates during heating and subsequent cooling: (a) 94, (b) 100, (c) 150, (d) 170, and (e) 200 °C during heating; (f) 30 °C during subsequent cooling. (g) In-plane scattering profiles extracted from the scattering pattern in (a) along the $2\theta_f$ direction at $\alpha_f = 0.165°$ and from the scattering patterns in (b–f) along the $2\theta_f$ direction at $\alpha_f = 0.133°$. (h) Out-of-plane scattering profiles extracted from the scattering patterns in (a–f) along the $\alpha_f$ direction at $2\theta_f = 0.462°$. In (g) and (h), the black symbols are the measured data and the red lines are the scattering profile obtained by fitting the measured data with the GIXS formula.

On the other hand, in the heating run the GISAXS pattern apparently varies very little in its intensity and shape up to 94 °C (Figure 5 and Figure S2). Thereafter, the scattering pattern has, however, changed somewhat in intensity and shape (Figure 5 and Figure S2). In particular, the scattering peaks have weakened and broadened significantly by 200 °C (Figure 5e,g,h). In the subsequent cooling from 200 °C, the scattering pattern is turned to enhance slightly in the intensity (Figure 5f–h). The measured GIXS patterns were analyzed in detail. The obtained structural parameters are listed in Table 1. In the heating run, the PE cylinders' dimension parameters ($d$, $R$, and $H$) and orientation retain almost unchanged below the melting transition of the PE crystals which is overlapped with the glass transition of the PMMA matrix. However, the structural parameters and orientation start to change slightly with temperature through the crystal melting and glass transitions (Table 1). Above the phase transition temperatures, they undergo further changes. The $d$ value increases to 19.2 nm at 150 °C and turns to drop very slightly to 19.0 nm at 170 °C, keeping the level until 190 °C. Then, the $d$ value further drops to 18.3 nm at 200 °C. The positional distortion factor $g$ value in the film plane always increases with increasing temperature, reaching to 0.197 at 200 °C. The $R$ value increases to 4.7 nm at 150 °C and stays at the level until 200 °C, while its $\sigma_R$ value also increases to 2.0 nm at 170 °C and stays at the level until 200 °C. In contrast, the $H$ value surprisingly drops with increasing temperature, reaching to 44.0 nm at 200 °C; its $\sigma_R$ value always increases, reaching to 11.8 nm at 200 °C. Here, the reductions with increasing temperature of the $H$ value are correlated to the expansions of the $R$ value. The mean polar angle $\overline{\varphi}$ is invariant with temperature changes. However, its $\sigma_\varphi$ value always increases with increasing temperature, reaching to 5.94° at 200 °C. These results collectively inform that the vertically oriented hexagonal cylinder structure formed in the diblock copolymer film is thermally stable below the PE crystal melting transition and the PMMA matrix' glass


dx.doi.org/10.1021/ma401440y | *Macromolecules* 2013, 46, 8235–8244

transition (which are overlapped in part). Then, the cylinder structure undergoes some variations in the structural dimension and orientation through the crystal melting and glass transition and further slight changes at higher temperatures but never collapses until 200 °C. These variations in the structural dimension and orientation above the crystal melting and glass transition temperatures might be attributed to the relatively high levels of the thermal motion of the block components and/or their segments in the PE cylinder phase as well as in the PMMA matrix phase. In the subsequent cooling run, all structural parameters and orientation are recovered somewhat from those at 200 °C but could not fully recover back to the original parameters and orientation before the heating. These again confirm that thermal annealing in a proper condition is required to build up a high-ordered hexagonal PE cylinder structure in the diblock copolymer thin film.

## CONCLUSIONS

An interesting crystalline−amorphous diblock copolymer $PE_{69}$-*b*-$PMMA_{92}$ was synthesized. This polymer was found to be stable up to 270 °C. The crystallization and the melting of the formed crystals in the PE block in the diblock copolymer were confirmed with DSC analysis. This PE crystal formation contributes to phase separation in the diblock copolymer, which consists of immiscible PE and PMMA blocks. However, the diblock copolymer was found to exhibit lower crystallization and melting temperatures than the PE homopolymer, which has a molecular weight similar to that of the PE block. Moreover, the overall crystallinity of the PE block phase was found to be only 10% of that of the PE homopolymer.

The morphological structures of the thermally annealed nanoscale thin films of the diblock copolymer were investigated in detail at various temperatures by using in-situ GIXS (GISAXS and GIWAXS) with a synchrotron radiation source. The quantitative GIXS analyses were used to reach the following conclusions about the structural details and their variations with temperature during heating and cooling. The PE and PMMA blocks were found to undergo phase separation and to form a hexagonally packed PE cylinder structure in the PMMA matrix in which the cylinders are preferentially oriented along a direction normal to the film plane. This hexagonal cylinder structure and its vertical orientation are well retained up to around 100 °C (which is the onset temperatures of PE crystal melting and PMMA glass transition). However, slight variations with temperature in the cylinders' dimensions and orientation were observed over 100−200 °C. The PE cylinders have a radius *R* of 4.3 nm and were found to undergo crystallization and crystal growth along a direction parallel to the cylinders' long axes. As a result, vertically grown lamellar crystals are developed in an orthorhombic lattice with *c*-axis in the film plane. Unfortunately, these vertically grown crystal lamellae are not well stacked because of the confinement effects of the limited space along the cylinders' short axes. Furthermore, the overall crystallinity of the PE cylinders is very low (only 14% of that of the PE homopolymer film). Overall, the analysis results show that the crystallization of the PE block chains in the copolymer thin film is severely restricted by the effects of confinement of the cylindrical geometry; there is only limited space for crystallization within the PMMA matrix and because of the limitations of the air and substrate interfaces and the anchoring in the diblock architecture of the chains to the cylindrical wall interface. In contrast, in a nanoscale thin film the PE homopolymer was demonstrated to form a highly ordered lamellar structure with lamellae well stacked along the out-of-plane of the film, even though the crystallization in the thin film is confined by the air and substrate interfaces. This well-ordered and oriented lamellar structural morphology cannot be achieved in melt-crystallized PE bulk specimens. These results show that the confinement effects in nanoscale thin films due to the air and substrate interfaces should not severely restrict PE crystallization.

## ASSOCIATED CONTENT

### Supporting Information

GIXS data analysis; Figures S1 and S2. This material is available free of charge via the Internet at http://pubs.acs.org.

## AUTHOR INFORMATION

### Corresponding Authors

*E-mail ree@postech.edu; Tel +82-54-279-2120; Fax +82-54-279-3399 (M.R.).

*E-mail kimsy@kaist.ac.kr; Tel +82-42-350-2834; Fax +82-42-350-2810 (S.Y.K.).

### Author Contributions

‖Y.Y.K., B.A., and S.S. contributed equally to this study.

### Notes

The authors declare no competing financial interest.

## ACKNOWLEDGMENTS

This study was supported by the National Research Foundation (NRF) of Korea (Doyak Program 2011-0028678, Center for Electro-Photo Behaviors in Advanced Molecular Systems (2008-0061892) and NRL program R0A-2008-000-20121-0) and the Ministry of Education (Global Excel Program and BK21 Plus Program). The synchrotron X-ray scattering measurements at the Pohang Accelerator Laboratory were supported by the Ministry of Science, ICT & Future Planning (MSIP), POSCO Company, and POSTECH Foundation.

## REFERENCES

(1) (a) Bates, F. S.; Fredrickson, G. H. *Annu. Rev. Phys. Chem.* **1990**, *41*, 525. (b) Liu, Y.; Zhao, W.; Zheng, X.; King, A.; Singh, A.; Rafailovich, M. H.; Sokolov, J.; Dai, K. H.; Kramer, E. J.; Schwarz, S. A.; Gebizlioglu, O.; Sinha, S. K. *Macromolecules* **1994**, *27*, 4000. (c) Mansky, P.; Russell, T. P.; Hawker, C. J.; Pitsikalis, M.; Mays, J. *Macromolecules* **1997**, *30*, 6810. (d) Park, M.; Harrison, C.; Chaikin, P. M.; Register, R. A.; Adamson, D. H. *Science* **1997**, *276*, 1401. (e) Krausch, G.; Magerle, R. *Adv. Mater.* **2002**, *14*, 1579.

(2) (a) Segalman, R. A.; Hexemer, A.; Kramer, E. J. *Macromolecules* **2003**, *36*, 6831. (b) Xu, T.; Goldbach, J. T.; Misner, M. J.; Kim, S.; Gibaud, A.; Gang, O.; Ocko, B.; Guarini, K. W.; Black, C. T.; Hawker, C. J.; Russell, T. P. *Macromolecules* **2004**, *37*, 2972. (c) Kim, S. H.; Misner, M. J.; Xu, T.; Kimura, M.; Russell, T. P. *Adv. Mater.* **2004**, *16*, 226. (d) Jeong, U.; Ryu, D. Y.; Kho, D. H.; Kim, J. K.; Goldbach, J. T.; Kim, D. H.; Russell, T. P. *Adv. Mater.* **2002**, *16*, 533. (e) Tung, S.-H.; Kalarickal, N. C.; Mays, J. W.; Xu, T. *Macromolecules* **2008**, *41*, 6453. (f) Park, S.; Lee, D. H.; Kim, B.; Hong, S. W.; Jeong, U.; Xu, T.; Russell, T. P. *Science* **2009**, *323*, 1030.

(3) (a) Fasolka, M. J.; Mayes, A. M. *Annu. Rev. Mater. Res.* **2001**, *31*, 323. (b) Park, C.; Yoon, J.; Thomas, E. L. *Polymer* **2003**, *44*, 6725. (c) Segalman, R. A. *Mater. Sci. Eng., R* **2005**, *48*, 191. (d) Olsen, B. D.; Segalman, R. A. *Mater. Sci. Eng., R* **2008**, *62*, 37. (e) Hamley, I. W. *Prog. Polym. Sci.* **2009**, *34*, 1161.

(4) (a) Ryan, A. J.; Hamley, I. W.; Bras, W.; Bates, F. S. *Macromolecules* **1995**, *28*, 3860. (b) Hong, S.; MacKnight, W. J.; Russell, T. P.; Gido, S. P. *Macromolecules* **2001**, *34*, 2398. (c) Hong, S.; MacKnight, W. J.; Russell, T. P.; Gido, S. P. *Macromolecules* **2001**, *34*, 2876. (d) Castillo, R. V.; Arnal, M. L.; Müller, A. J.; Hamley, I. W.; Castelletto, V.; Schmalz, H.; Abetz, V. *Macromolecules* **2008**, *41*, 879. (e) Lemstra, P. J. *Science*

**2009**, *323*, 725. (f) Wang, H.; Keum, J. K.; Hiltner, A.; Baer, E.; Freeman, B.; Rozanski, A.; Galeski, A. *Science* **2009**, *323*, 757.

(5) (a) Hamley, I. W.; Fairclough, J. P. A.; Ryan, A. J.; Bates, F. S.; Towns-Andrews, E. *Polymer* **1996**, *37*, 4425. (b) Nojima, S.; Kato, K.; Yamamoto, S.; Ashida, T. *Macromolecules* **1992**, *25*, 2237. (c) Hamley, I. W.; Fairclough, J. P. A.; Terrill, N. J.; Ryan, A. J.; Lipic, P. M.; Bates, F. S.; Towns-Andrews, E. *Macromolecules* **1996**, *29*, 8835. (d) Kim, G.; Han, C. C.; Libera, M.; Jackson, C. L. *Macromolecules* **2001**, *34*, 7336. (e) Hsiao, M.-S.; Chen, W. Y.; Zheng, J. X.; Van Horn, R. M.; Quirk, R. P.; Ivanov, D. A.; Thomas, E. L.; Lotz, B.; Cheng, S. Z. D. *Macromolecules* **2008**, *41*, 4794. (f) Wang, H.; Keum, J. K.; Hiltner, A.; Baer, E. *Macromolecules* **2010**, *43*, 3359.

(6) (a) Zhu, L.; Cheng, S. Z. D.; Calhoun, B. H.; Ge, Q.; Quirk, R. P.; Thomas, E. L.; Hsiao, B. S.; Yeh, F.; Lotz, B. *J. Am. Chem. Soc.* **2000**, *122*, 5957. (b) Zhu, L.; Cheng, S. Z. D.; Calhoun, B. H.; Ge, Q.; Quirk, R. P.; Thomas, E. L.; Hsiao, B. S.; Yeh, F.; Lotz, B. *Polymer* **2001**, *42*, 5829. (c) Huang, P.; Zhu, L.; Guo, Y.; Ge, Q.; Jing, A. J.; Chen, W. Y.; Quirk, R. P.; Cheng, S. Z. D.; Thomas, E. L.; Lotz, B.; Hsiao, B. S.; Avila-Orta, C. A.; Sics, I. *Macromolecules* **2004**, *37*, 3689. (d) Sun, L.; Zhu, L.; Ge, Q.; Quirk, R. P.; Xue, C.; Cheng, S. Z. D.; Hsiao, B. S.; Avila-Orta, C. A.; Sics, I.; Cantino, M. E. *Polymer* **2004**, *45*, 2931. (e) Huang, P.; Guo, Y.; Quirk, R. P.; Ruan, J.; Lotz, B.; Thomas, E. L.; Hsiao, B. S.; Avila-Orta, C. A.; Sics, I.; Cheng, S. Z. D. *Polymer* **2006**, *47*, 5457. (f) Huang, P.; Zheng, J. X.; Leng, S.; Van Horn, R. M.; Jeong, K.-U.; Guo, Y.; Quirk, R. P.; Cheng, Z. D.; Lotz, B.; Thomas, E. L.; Hsiao, B. S. *Macromolecules* **2007**, *40*, 526.

(7) (a) Yu-Su, S. Y.; Sheiko, S. S.; Lee, H.; Jakubowski, W.; Nese, A.; Matyjaszewski, K.; Anokhin, D.; Ivanov, D. A. *Macromolecules* **2009**, *42*, 9008. (b) Yang, P.; Yu, X.; Han, Y. *Polymer* **2010**, *51*, 4948. (c) Zhao, J.; Zhang, J.; Duan, X.; Peng, Z.; Wang, S. *Polymer* **2011**, *52*, 2085. (d) Fu, J.; Wei, Y.; Xue, L.; Luan, B.; Pan, C.; Li, B.; Han, Y. *Polymer* **2009**, *50*, 1588. (e) Yang, P.; Han, Y. *Macromol. Rapid Commun.* **2008**, *29*, 1614.

(8) (a) Gamboa, A. L. S.; Filipe, E. J. M.; Brogueira, P. *Nano Lett.* **2002**, *2*, 1083. (b) Knobler, C. M.; Schwartz, D. K. *Curr. Opin. Colloid Interface Sci.* **1999**, *4*, 46. (c) Rapaport, H.; Kjaer, K.; Jensen, T. R.; Leiserowitz, L.; Tirrel, D. A. *J. Am. Chem. Soc.* **2000**, *122*, 12523.

(9) (a) Han, C. J.; Lee, M. S.; Byun, D.-J.; Kim, S.-Y. *Macromolecules* **2002**, *35*, 8923. (b) Matsugi, T.; Kojoh, S.-I.; Kawahara, N.; Matsuo, S.; Kaneko, H.; Kashiwa, N. *J. Polym. Sci., Part A: Polym. Chem.* **2003**, *41*, 3965. (c) Inoue, Y.; Matyjaszewski, M. *J. Polym. Sci., Part A: Polym. Chem.* **2004**, *42*, 496. (d) Jeon, M. Ph.D. Thesis, Korea Advanced Institute of Science and Technology, 2008.

(10) (a) Yoon, J.; Kim, K.-W.; Kim, J.; Heo, K.; Jin, K. S.; Jin, S.; Shin, T. J.; Lee, B.; Rho, Y.; Ahn, B.; Ree, M. *Macromol. Res.* **2008**, *16*, 575. (b) Bolze, J.; Kim, J.; Huang, J.-Y.; Rah, S.; Youn, H. S.; Lee, B.; Shin, T. J.; Ree, M. *Macromol. Res.* **2002**, *10*, 2. (c) Yoon, J.; Choi, S.; Jin, S.; Jin, K. S.; Heo, K.; Ree, M. *J. Appl. Crystallogr.* **2007**, *40*, s669. (d) Yoon, J.; Jin, K. S.; Kim, H. C.; Kim, G.; Heo, K.; Jin, S.; Kim, J.; Kim, K.-W.; Ree, M. *J. Appl. Crystallogr.* **2007**, *40*, 476. (e) Yoon, J.; Lee, S. W.; Choi, S.; Heo, K.; Jin, K. S.; Jin, S.; Kim, G.; Kim, J.; Kim, K.-W.; Kim, H.; Ree, M. *J. Phys. Chem. B* **2008**, *112*, 5338.

(11) (a) Yoon, J.; Jung, S. Y.; Ahn, B.; Heo, K.; Jin, S.; Iyoda, T.; Yoshida, H.; Ree, M. *J. Phys. Chem. B* **2008**, *112*, 8486. (b) Yoon, J.; Jin, S.; Ahn, B.; Rho, Y.; Hirai, T.; Maeda, R.; Hayakawa, T.; Kim, J.; Kim, K.-W.; Ree, M. *Macromolecules* **2008**, *41*, 8778. (c) Jin, S.; Hirai, T.; Ahn, B.; Rho, Y.; Kim, K.-W.; Kakimoto, M.; Gopalan, P.; Hayakawa, T.; Ree, M. *J. Phys. Chem. B* **2010**, *114*, 8033. (d) Ahn, B.; Hirai, T.; Jin, S.; Rho, Y.; Kim, K.-W.; Kakimoto, M.; Gopalan, P.; Hayakawa, T.; Ree, M. *Macromolecules* **2010**, *43*, 10568.

(12) Blaine, R. L. Technical Note #48: "Polymer Heats of Fusion", TA Instruments. New Castle, DE.

(13) (a) Lee, B.; Park, Y.-H.; Hwang, Y.; Oh, W.; Yoon, J.; Ree, M. *Nat. Mater.* **2005**, *4*, 147. (b) Kim, G.; Yoon, J.; Kim, J.-S.; Kim, H.; Ree, M. *J. Phys. Chem. B* **2008**, *112*, 8868.

(14) (a) Jin, S.; Yoon, J.; Heo, K.; Park, H.-W.; Shin, T. J.; Chang, T.; Ree, M. *J. Appl. Crystallogr.* **2007**, *40*, 950. (b) Heo, K.; Yoon, J.; Jin, S.; Kim, J.; Kim, K.-W.; Shin, T. J.; Chung, B.; Chang, T.; Ree, M. *J. Appl. Crystallogr.* **2008**, *41*, 281. (c) Ahn, B.; Kim, D. M.; Hsu, J.-C.; Ko, Y.-G.; Shin, T. J.; Kim, J.; Chen, W.-C.; Ree, M. *ACS Macro Lett.* **2013**, *2*, 555. (d) Rho, Y.; Min, J.; Yoon, J.; Ahn, B.; Jung, S.; Kim, K.; Shah, P.; Lee, J.-S.; Ree, M. *NPG Asia Mater.* **2012**, *4*, e29.

(15) Lee, B.; Park, I.; Yoon, J.; Park, S.; Kim, J.; Kim, K.-W.; Chang, T.; Ree, M. *Macromolecules* **2005**, *38*, 4311.

(16) (a) Yang, S. Y.; Park, J.; Yoon, J.; Ree, M.; Jang, S. K.; Kim, J. K. *Adv. Funct. Mater.* **2008**, *18*, 1371. (b) Yoon, J.; Yang, S. Y.; Heo, K.; Lee, B.; Joo, W.; Kim, J. K.; Ree, M. *J. Appl. Crystallogr.* **2007**, *40*, 305.

(17) (a) Mansky, P.; Liu, Y.; Huang, E.; Russell, T. P.; Hawker, C. *Science* **1997**, *275*, 1458. (b) Wang, Q.; Nealey, P. F.; de Pablo, J. J. *Macromolecules* **2001**, *34*, 3458.

(18) (a) Starkweather, H. W., Jr. *Polym. Eng. Sci.* **1965**, *5*, 5. (b) Fowke, F. M. *J. Adhes. Sci. Technol.* **1987**, *1*, 7.

(19) (a) Wu, S. *J. Phys. Chem.* **1970**, *74*, 632. (b) van Oss, C. J.; Good, R. J.; Busscher, H. J. *J. Dispersion Sci. Technol.* **1990**, *11*, 75.

(20) Miskiewicz, P.; Kotarba, S.; Jung, J.; Marszalek, T.; Mas-Torrent, M.; Gomar-Nadal, E.; Amabilino, D. B.; Rovira, C.; Veciana, J.; Maniukiewicz, W.; Ulanski, J. *J. Appl. Phys.* **2008**, *104*, 054509.

(21) Lide, D. R. *CRC Handbook of Chemistry and Physics*, 89th ed.; CRC: Boca Raton, FL, 2009.

(22) (a) Brandrup, J.; Immergut, E. H. *Polymer Handbook*, 3rd ed.; John Wiley & Sons: New York, 1989. (b) Tadokoro, H. *Structure of Crystalline Polymers*; Robert E. Krieger: Malabar, FL, 1990. (c) Jiang, Z.; Tang, Y.; Rieger, J.; Enderle, H.-F.; Lilge, D.; Roth, S. V.; Gehrke, R.; Wu, Z.; Li, Z.; Men, Y. *Polymer* **2009**, *50*, 4101. (d) Shin, T. J.; Lee, B.; Seong, B. S.; Han, Y. S.; Lee, C.-H.; Song, H. H.; Stein, R. S.; Ree, M. *Polymer* **2010**, *51*, 5799. (e) Shin, T. J.; Lee, B.; Lee, J.; Jin, S.; Sung, B. S.; Han, Y. S.; Lee, C.-H.; Stein, R. S.; Ree, M. *J. Appl. Crystallogr.* **2009**, *42*, 161. (f) Song, H. H.; Ree, M.; Wu, D. Q.; Chu, B.; Satkowski, M.; Stein, R. S.; Phillips, J. C. *Macromolecules* **1990**, *23*, 2380. (g) Song, H. H.; Wu, D. Q.; Ree, M.; Stein, R. S.; Phillips, J. C.; LeGrand, A.; Chu, B. *Macromolecules* **1988**, *21*, 1180.